Physical, Mechanical, and Conductivity Properties of Poly(3-hexylthiophene)−Montmorillonite Clay Nanocomposites Produced by the Solvent Casting Method

Biplab K. Kuila and Arun K. Nandi*

Polymer Science Unit, Indian Association for the Cultivation of Science, Jadavpur, Kolkata 700 032, India

Received May 14, 2004; Revised Manuscript Received September 7, 2004

ABSTRACT: Polymer nanocomposites (PNCs) of poly(3-hexylthiophene) (P3HT) with organically modified montmorillonite (om-MMT) clay have been prepared by the solvent casting method. WAXS and TEM studies indicate exfoliated clay structure for lower clay content, but at higher clay content (5%, w/w) intercalated structures appear. The interchain lamella of P3HT exists in the nanocomposite, and the P3HT crystals become more ordered, showing better X-ray diffraction peaks. The thermal stability of PNCs increases significantly, and 1% clay content PNC exhibits the maximum thermal stability. The glass transition temperature (T_g), β-transition temperature (T_β), the melting point (T_m), and the enthalpy of fusion (ΔH) of the PNCs are increased as compared to those of pure P3HT. The storage modulus (G') of PNCs showed a dramatic increase from that of pure P3HT, and the increase is larger in the temperature range 20−50 °C. The FTIR study indicates a decrease in Si−O−Si and Si−O stretching frequency for the exfoliated clay structure. The UV−vis study showed a blue shift of the $\pi-\pi^*$ transition band of P3HT in the PNCs, and they exhibit photoluminescence quenching which increases with increase in clay concentration. The dc conductivity of undoped PNCs remains almost the same as that of pure P3HT, but iodine-doped PNCs, however, exhibit 2.5−3 times greater conductivity than that of iodine-doped P3HT.

Introduction

Poly(3-hexylthiophene) (P3HT) is an important conducting polymer because of its excellent electrical conductivity, electroluminescence, and nonlinear optical properties.[1] However, its physical, thermal, and mechanical properties are not very good and finds difficulties in many applications. Recently, polymer−clay nanocomposites (PNCs) have received significant research attention for the large-scale improvement in the mechanical and physical properties.[2−7] The large interfacial area and the nanoscopic dimension of the clay nanoparticles in the polymer matrix yield such a dramatic improvement.[2] To improve the physical and mechanical properties of this important conducting polymer, we attempted to make P3HT−clay nanocomposites, and here we report the preparation, characterization, and properties of these nanocomposites. The conductivity and optical properties of a conducting polymer depend mainly on the arrangement of its chains. The clay nanoparticales may influence the arrangement of P3HT chains, as it may become confined into the clay tactoids. So some variation of the above properties in the nanocomposites is expected. Certainly, a useful product may come out by a combination of good mechanical, thermal, and conductivity properties.

Montmorillonite (MMT) is a clay mineral consisting of stacked silicate sheets (thickness ∼1 nm, length ∼218 nm) with high aspect ratio (220) and with a platelike morphology.[8] This high aspect ratio (ratio of length to thickness) plays an important role for the enhancement of mechanical and physical properties. Chemically, MMT consists of two fused silicate tetrahedral sheets sandwiching an edge-shared octahedral sheet of either magnesium or aluminum hydroxide. In the interlayer region there exists Na^+ and Ca^{2+}, which can be replaced by the alkylammonium and alkylphosphonium ions rendering the clay into organophilic nature.[2,3,9] The organic modifier plays an important role for producing the nanocomposite. It may either enhance the interaction between the clay and the polymer, making it more suitably mixed, or it may favor the intercalation of the polymer chain by dictating the gallery spacing. Pure P3HT is a comblike polymer having a pendent hexyl group with interchain lamella structure (Scheme 1). Depending on the extent of interdigitation of the hexyl groups, two types of P3HT crystals are produced.[10] Type I crystals are produced by casting the P3HT film from its *m*-xylene solution very fast at 60 °C or by melt quenching, and type II crystals are produced by casting the film from the same solution slowly (1−2 days). During the preparation of PNCs the pendent hexyl group may interact with the organic modifier of the clay and make the clay easily dispersed into it. The P3HT interchain lamella may or may not change during such mixing (Scheme 1). Thus, there is a possibility of hierarchical structure for the presence of P3HT lamella into the clay lamella. Depending on the penetration of the polymer matrix into the silicate galleries of the organically modified clay, various structures from intercalated to exfoliated may be produced. Certainly these different structures of the composite would yield newer physical and mechanical properties of this important conducting polymer. The entrapment of conducting polymer chains within the silicate layers may have important consequences, and some study has been recently reported for the polymer polyaniline (PANI)[11−16] and polypyrrole (PPY).[17] Various methods have been used to synthesize the PANI−MMT clay nanocomposite, e.g., sol−gel method, emulsion polymerization, electropolymerization, etc., and the properties were found to be dependent on the preparation procedure. Dode-

* Corresponding author: e-mail psuakn@mahendra.iacs.res.in.

10.1021/ma0490496 CCC: $27.50
Published on Web 10/16/2004

Scheme 1. Schematic Models of Two Types of Lamellar Crystals of P3HT[a]

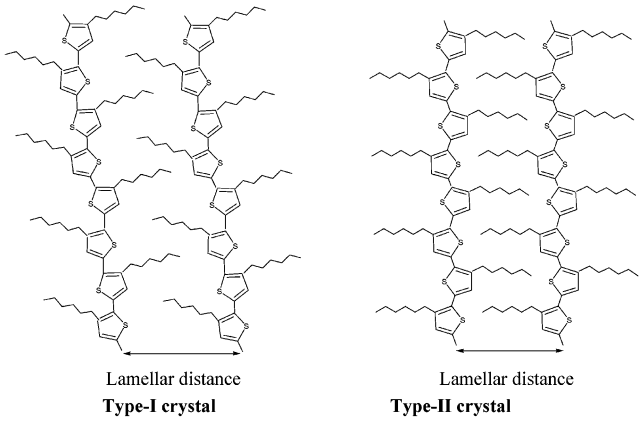

[a] Type I has a tilt on the polymer chain but type II polymer chain is planar with a good interdigitation of hexyl groups.[10]

cylbenzenesulfonic acid (DBSA)-doped PANI−clay nanocomposite exhibited lower conductivity than that of DBSA-doped PANI, the former exhibited the insulating region while the latter exhibits the metallic region in the temperature range 10−170 K.[14] The low-conductivity state of the PANI-DBSA/clay system originates from the resistivity due to insertion of clay layer. The PANI−MMT composites exhibited better thermal stability, anticorrosion performance, and larger reduction in gas permeability than those in conventional PANI.[11,12] Clay platelets hinder the diffusion of oxygen/air within the composite, causing increased thermal stability and reduction in gas permeability. Some enhancement in conductivity and thermal stability is recently achieved in PNCs of electropolymerized PPY and caprolactum-modified clay.[17] The clay platelets provide an environment for the initial growth of ordered PPY films, and the subsequent growth is not intercalative but by simply coated on the platelet surface, causing higher conductivity. Both photoluminescence and electroluminescence efficiency are enhanced in poly[2-methoxy-5-(2′-ethylhexyloxy)-1,4-phenylenevinylene] (MEH−PPV)/clay nanocomposite compared to that of pure MEH−PPV.[18] The enhancement of photoluminescence property has been attributed for the reduction of interchain interaction and isolating the conjugated polymer chains within a confined geometry, thereby preventing exitons from finding the lower energy trap. Therefore, improvement in the physical properties of conducting polymers has been achieved by making the PNCs. However, no study is yet been reported on the important conducting polymer polythiophene. Polythiophene is insoluble and infusible, so it is difficult to process.[19] Consequently, P3HT has been chosen, as it is both fusible and soluble.[19,20] So both the processes of solution mixing and melt mixing can be applied to produce the PNCs, and here we report the process of solution mixing to make the PNCs. The main objective of this work is to improve mechanical and physical properties of P3HT without lowering the conductivity. So the material may find its uses in various electronic applications where good mechanical property and thermal stability are required. Also, the absorption and photoluminescence spectra of this system have been studied to understand any change in chain conformation and its relation with conductivity. Here regioirregular P3HT has been used to prepare the PNCs.

Experimental Section

(a) Samples. P3HT (regioirregular) was synthesized from the monomer hexylthiophene that was prepared from 3-bromothiophene and *n*-hexyl bromide using a Grignard reaction. It was purified by passing petroleum ether solution through a silica gel column.[20] The polymer was synthesized in $CHCl_3$ medium using anhydrous $FeCl_3$ as initiator under a nitrogen atmosphere.[21] The polymerization was carried out at 0 °C for 24 h, and then the reaction mixture was poured into methanol containing 10% (v/v) 12 N HCl. The precipitate was washed with methanol and dissolved in chloroform. It was then filtered, and the solution was dried in air and finally in a vacuum at 60 °C for 3 days. The head−tail (H−T) regioregularity of the sample was measured from ^{1}H NMR spectra in $CDCl_3$[21] and was found to be 82 mol %. The molecular weight ($\overline{M}_w$) of the sample was measured by gel permeation chromatography (GPC; Waters) using $CHCl_3$ as solvent and polystyrene as standard. The characteristics of the samples are presented in Table 1.

The MMT clay (PGV-PV-178-00) is a product of Nanocor, Arlington Height, IL, was organically modified using cetyltrimethylammonium bromide (CTAB).[22] The MMT clay was dispersed in water, and CTAB was added in the ratio 2:1 by weight. It was then stirred for 12 h. The modified clay was collected by centrifugation (9000 rpm). Excess CTAB was removed by repeated centrifugation with water while monitoring the removal of bromide ion with $AgNO_3$ test. Then it was dried in a vacuum at 60 °C for 3 days. The exchange capacity of the clay was measured by thermogravimetric analysis (TGA) of organically modified MMT (om-MMT) clay by heating it from 30 to 800 °C under a nitrogen atmosphere in a Simadzu TGA instrument (model TGA-50).[23] The weight loss by heating Na^+-MMT clay from 30 to 800 °C was used to obtain the amount of absorbed water and structural water present in the clay. In our sample the thermogram from 30 to 120 °C indicates a weight loss of 9.37% while that from 120 to 800 °C indicates a weight loss of 5.02% (Figure 1 of Supporting Information). The former is the absorbed moisture, and the latter is the structural water present in the clay. The weight loss of om-MMT from 120 to 800 °C was 34.23%, so the weight loss due to cetyltrimethylammonium (CTA) ion is 29.21% and is equal to 101.4 mequiv/100 g (equiv wt of CTA ion 288). This is the exchange capacity of the clay used in the work.

(b) Preparation of Nanocomposite. The nanocomposite of the organically modified MMT clay was prepared by the solution casting method. The clay was first dispersed in chloroform (12.5×10^{-5} g cm^{-3}) by sonication in an ultrasonic bath (60 W, model AVI0C, Eyela) operating at 28 kHz frequency for 30 min. P3HT (2.5×10^{-3} g cm^{-3}) was then added and stirred at 40 °C for 3 h. Chloroform was dried off by evaporation and was finally dried in a vacuum at 60 °C for 3 days. The nanocomposites are designated as PNC1, PNC2.5, and PNC5; the number at the right-hand side indicates the clay percentage (w/w).

(c) Wide-Angle X-ray Scattering. The WAXS experiments were done on the above solvent cast films. The experiments were carried out in a Seifert X-ray diffractometer (C 300) in reflection mode with a parallel beam optics attachment. The instrument was operated at a 35 kV voltage and a 30 mA current and was calibrated with a standard silicon sample. Nickel-filtered copper Kα radiation ($\lambda = 0.154$ nm) was used in the work. The samples were scanned from $2\theta = 2°$ to 45° at the step scan mode (step size 0.03°, preset time 2 s), and the diffraction pattern was recorded using a scintillation counter detector.

(d) Transmission Electron Microscopy (TEM). The dispersity of the clay particles into the polymer matrix was studied using a TEM (Philips C M 200) operated at an accelerated voltage of 200 kV without staining. A thin section (~80 nm) of the above nanocomposite was made by encapsulating it in an epoxy matrix and cutting at 25 °C through a ultra-cryomicrotome (Ultracut R, Leica) equipped with a glass knife. It was then placed on copper grid and was observed through the microscope.

(e) Thermal Measurement. A Perkin-Elmer DSC-7 fitted with Intracooler-1 and working under a nitrogen atmosphere was used in this work. It was calibrated with indium before each set of experiment. About 3 mg samples were taken in aluminum pans and were sealed by a quick press. They were heated at the scan rate of 10 °C/min from −30 to 230 °C. The melting temperature (peak temperature) and enthalpy of melting were measured.

The thermogravimetric analysis (TGA) experiments were made using a Mettler Toledo TGA/(SDTA851e) instrument under a N_2 atmosphere at a heating rate of 10 °C/min.

(f) Dynamical Mechanical Property Measurements. The mechanical properties of the polymers were measured using a dynamic mechanical analyzer (DMA) (TA Instruments, model Q-800). Films of 25 mm × 5 mm × 0.15 mm dimensions were made from the composites by solution casting on a die, and they were installed in the tension clamp of the calibrated instrument. The samples were heated from −130 to 100 °C at a heating rate of 10 °C/min. The storage modulus, loss modulus, and tan δ were measured at constant frequency of 10 Hz with a static force of 0.02 N.

(g) dc Conductivity Measurement. The dc conductivity of the samples at 30 °C were measured by the standard spring-loaded pressure contact four-probe method.[24] A circular film of 1.3 cm diameter was used. A constant current (I) was passed from a constant direct current source electrometer (Keithley model 617) through two adjacent leads of the four probes, and the voltage (V) across the other two leads was measured using a multimeter (Keithley, model 2000). The conductivity (σ) was calculated using the van der Paw relation

$$\sigma = (\ln 2/\pi d)(I/V) \quad (1)$$

where d, the thickness of the film, was taken as the average of four measurements at different places using a screw gauge. Conductivity of two films of same sample, each with two trials, was measured, and the average of four such measurements yields the conductivity value.

(h) Spectroscopy. The UV−vis spectra of the P3HT−clay nanocomposite films were studied by casting the films on quartz plates and drying at 60 °C in a vacuum for 2 days. The spectra were taken against air from 200 to 1000 nm in an UV−vis spectrophotometer (Hewlett-Packard, model 8453) at 30 °C. The photoluminescence spectra of the samples were measured in a Perkin-Elmer instrument (LS55 Luminescence spectrometer) on solvent cast films. The photoexcitation at 490 nm was performed at a 45° angle of the thin film plane, and the emission was detected at a right angle with respect to the excitation beam direction. Each spectrum was normalized with film thickness of one micrometer for comparison purposes. The FT-IR spectra of the samples were performed from the films in a Nicolet FT-IR instrument [Magna-1R-750 spectrometer (series-11)].

Results and Discussion

WAXS Pattern and TEM Observation. Figure 1 shows the WAXS patterns of MMT clay, organically modified clay, P3HT, and P3HT−MMT composites at different MMT concentrations. It is clear from the figure that in organically modified clay (om-MMT) the lamella peak shifted to a lower 2θ value compared to that of unmodified clay. This is similar to those observed in previous works.[4,25] Here the gallery spacing of MMT shifts from 1.33 to 2.01 nm. The increase in gallery spacing is due to the incorporation of cetyl chains of CTAB into the gallery replacing the Na^+ and Ca^{2+}. This certainly indicates that the MMT clay became organically modified. From the P3HT diffractrogram (diffractrogram C) it is clear that P3HT has interchain lamellar structure with lamellar thickness 1.73 nm.[20] The interchain lamellar structure is produced due to the side chain ordering as shown in Scheme 1. In the nanocomposites (PNC1 and PNC2.5) this P3HT interchain lamellar peak occurs at some higher angle ($2\theta = 5.24°$); i.e., the interchain lamellar length decreased by 0.05 nm. The absence of lamellar peak at 2.01 nm indicates that the MMT clay becomes totally exfoliated. In the PNC5 sample apart from the main peak at $2\theta = 5.09°$ there are two humps at $2\theta = 4.4°$ and 3.5° (judged from enlarging the X-ray pattern, inset of the figure). These correspond to d spacings of pure polymer, om-clay (2.01 nm), and a new lamellar thickness (2.52 nm), respectively. The new lamellar structure may be produced due to expansion of clay lamella for the intercalation of P3HT lamella (thickness 1.73 nm). In such a case hierarchical structure (P3HT lamella within clay lamella: i.e., a superstructure within other superstructure) is produced. The intercalation of P3HT lamella may not be limited to a single P3HT lamella; multiple P3HT lamella may also be intercalated. Because of the limitation of our X-ray apparatus to work at lower angles, we could not ascertain other lower angle peaks.

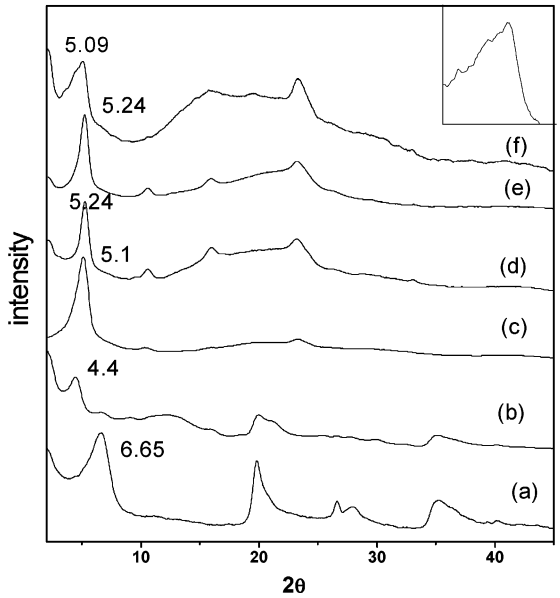

Figure 1. WAXS patterns of MMT−P3HT clay nanocomposites: (a) pure clay, (b) organically modified clay, (c) P3HT, (d) PNC1, (e) PNC2.5, and (f) PNC5. Inset: enlarged portion of diffractogram (f) at lower diffraction angle (2−7°).

An interesting observation is that the crystalline diffraction peak of P3HT ($2\theta = 23.2°$) becomes more distinct in the PNCs; probably crystals become more ordered here. The X-ray diffraction peak positions and their normalized intensities with respect to their lamellar peak (I/I_0) are presented in Table 2. It is apparent that the peak positions of PNCs (except the lamellar peak) are the same with that of pure P3HT, indicating P3HT unit cell structure remains unaffected in the PNCs. The crystal structure of P3HT is reported by many workers,[10,26] and there exists two types of P3HT crystals (type 1 and type 2), depending upon the orientation of the side chain along the main chain.[10] The increased I/I_0 values of all the diffraction peaks for the PNCs in comparison with those of pure P3HT supports that the P3HT crystals became more ordered in the PNCs. The X-ray diffraction pattern of P3HT and the PNCs clearly indicate the formation of type 1 crystals.[10,20] Here the overlap (interdigitation) between the side chains in neighboring stacks is minimal although there can be ordering of the side chains across the layer−layer interface.[10] With addition of clay some more

Table 1. Characteristics of the Samples

poly(3-hexylthiophene) (P3HT)	montmorillonite clay data from Nanocor, Inc. PGV; PV-178-00
product: synthesized	product: Nanocor, Inc. USA
H−T regioregularity: 82%	color: white
$\overline{M}_w$: 111200	cation exchange
polydispersity index (PDI): 1.78	capacity (mequiv/100 g): 101.4[a]
melting temperature: 189 °C	aspect ratio: 150−200
	specific gravity: 2.6

[a] Measured value using TGA.

Table 2. Peak Positions, Lamella Thickness, and I/I_0 of Different XRD Peaks of P3HT in the Nanocomposites[a]

sample	lamellar distance (nm)	I_0 (height in cm)	I/I_0 at different peak positions (2θ) 10.36 (0.853 nm)	15.9 (0.557 nm)	23.25 (0.382 nm)
P3HT	1.73	7.2	0.04	0.04	0.13
PNC1	1.68	5.8	0.16	0.48	0.61
PNC2.5	1.68	9.6	0.11	0.26	0.49
PNC5	2.52	3.9	0.10	0.73	0.95
	1.99				
	1.73				

[a] I_0 is the intensity (height from baseline) of P3HT interchain lamellar peak in each diffractogram. Figures in parentheses indicate the d values.

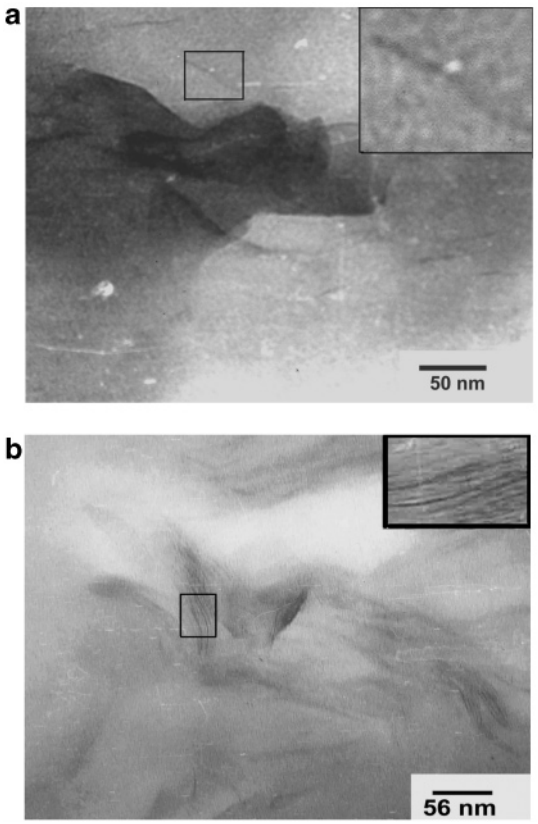

Figure 2. TEM micrographs of MMT clay−P3HT nanocomposites: (a) PNC2.5 (inset 3 times enlargement of box mark); (b) PNC5 (inset 3 times enlargement of box mark).

interdigitation takes place, decreasing the interchain lamellar spacing for PNC1 and PNC2.5 sample (Table 2).

To substantiate the X-ray results, we made a TEM study of the samples, and the TEM micrographs are presented in Figure 2a,b. It is clear from the micrographs that PNC2.5 has exfoliated structure as there are no parallel stacks of clay platelets; rather, there are angular dispositions of clay platelets with average

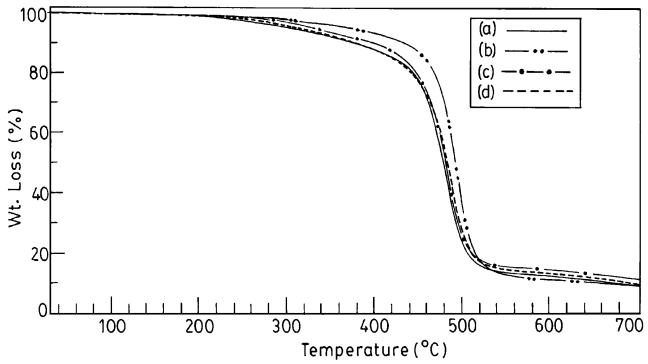

Figure 3. TGA thermograms of P3HT and PNCs under a N_2 atmosphere at 10 °C/min heating rate: (a) P3HT, (b) PNC1, (c) PNC2.5, and (d) PNC5.

distance larger than 10 nm. But in the PNC5 there are parallel stacks of clay lamella (dark contrast) supporting intercalated structure. When the micrographs are examined with a peak scale lupe (7×) lamella distances of 2.2, 2.8, and 5.6 nm are observed for the black contrast clay lamella, indicating multiple intercalation of P3HT lamella into the clay lamella. The P3HT lamella are also observed through the peak scale lupe (7×) (gray contrast) or by enlargement of TEM pictures[27] (Figure 2, Supporting Information), and single to three such lamella intercalation was observed between two clay lamella (inset of Figure 2b). Thus, hierarchical structure is produced for the PNC5 sample. In the PNC2.5 sample the P3HT lamella, observed through the peak scale lupe(7×) or by enlargement, are not straight and parallel as in PNC5; rather, many folds within the P3HT strands (e.g., 60° fold, 120° fold, hairpin fold, etc.) are observed.[27] As a result, they are not in parallel position to the clay tactoids, but they are mostly at different angles to the tactoids. The average distance between the clay platelets is about 15 nm, and the clay platelets are not parallel to each other. So the clay platelets are exfoliated in PNC2.5, and multiple clay platelets also coexist with individual silicate layers.[11] The frequent folding of P3HT strands may allow the hexyl side chains to interdigitate more, giving higher crystallinity and also a small decrease in lamellar thickness (cf. DSC and X-ray results).

Thermogravimetric Analysis. Figure 3 shows the typical TGA thermograms of weight loss as a function of temperature of P3HT and the PNCs as measured under a N_2 atmosphere. It is apparent from the figure that all the PNCs have greater thermal stability than that of pure P3HT and the PNC1 has the highest. The degradation temperature as measured from the intersection of the tangent of the initial part and the inflection part are 428.6, 456, 437.1, and 437.1 °C for pure P3HT, PNC1, PNC2.5, and PNC5, respectively. The reason for the dramatic increase in thermal stability of PNC1 is not known, but it might be attributed to the more ordered crystal (cf. DSC results) of P3HT at this composite composition. It is suggested that in the PNCs the clay particles act as barriers due to their high aspect ratio and thereby hinder the degradation process.

Differential Scanning Calorimetry. In Figure 4 the DSC thermograms of pure P3HT and P3HT−MMT nanocomposites (as prepared) are presented. It is clear from the thermograms that PNC1 and PNC2.5 exhibit 10 and 5 °C higher melting point (T_m) than that of pure P3HT, but the PNC5 exhibits almost same melting point as that of pure P3HT. The enthalpy of fusion (ΔH)

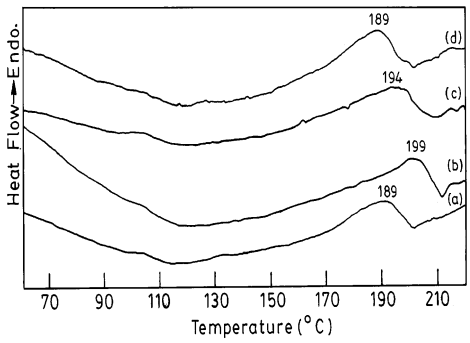

Figure 4. DSC thermograms of the P3HT−PNCs: (a) P3HT, (b) PNC1, (c) PNC2.5, and (d) PNC5.

values are 7.0, 6.1, 5.9, and 4.5 J/g for PNC1, PNC2.5, PNC5, and pure P3HT, respectively. Thus, in PNC1 and PNC2.5 both melting point and enthalpy showed an increase indicating better crystal formation, supporting the increased intensity of X-ray peaks. The reason for larger increase of melting point and enthalpy of fusion of PNC1 and PNC2.5 compared to those of PNC 5 and P3HT is not clear to us. It may be proposed that 1% omMMT clay produce good dispersion in the solution, thereby helping the crystallization of P3HT by nucleation and growth processes to produce more ordered crystal. At higher percentage of clay it may not be so highly dispersed. At these compositions also the exfoliated clay tactoids are at different angles to the P3HT lamella. It might be probable that such an arrangement of dispersed clay tactoids for their cohesive force of attraction decreases the tilt of the P3HT side chains (Scheme 1) and helps the side chains to interdigitate more (Table 2), yielding an increased crystallinity and melting point. But clay lamellas parallel to the P3HT strands do not influence to decrease the tilt of side chains, and as a result the crystallinity, melting point, and the interchain lamellar distance remain unchanged for the PNC5 sample.

Mechanical Properties. Figure 5a−c shows the temperature dependence of storage modulus, loss modulus, and tan δ of P3HT and of three PNCs. The storage or elastic modulus (G') relates the ability of the material to store or return energy when oscillatory force is applied to the specimen, and the loss modulus (G'') relates the ability to lose the energy. From Figure 5a it is apparent that with increase in temperature storage modulus decreases, and at about 100 °C it is negligibly small for all the samples. The storage modulus of all P3HT−clay nanocomposite increased than that of pure P3HT. In these thermograms there are two breaks one at lower temperature (∼−100 °C) and the other at higher temperature (∼20 °C), indicating two different types of transitions in the P3HT chains. It is clearer in Figure 5b where the loss modulus is plotted with temperature. There are two peaks in every sample; both the peak temperatures increased with increasing clay content. The lower temperature peak (T_β) may arise from the β transition (i.e., relaxation of hexyl side chains) while the higher temperature peak may arise from the α transition (i.e., relaxation of the main chain).[28,29] The latter may be described as the glass transition temperature (T_g), and both transition temperatures are presented in Table 3. The results show a remarkable increase in T_g (∼40 °C) for the PNCs, but the β transition temperature's increase is much lower (5−17 °C). So it appears that the effect of clay nano-

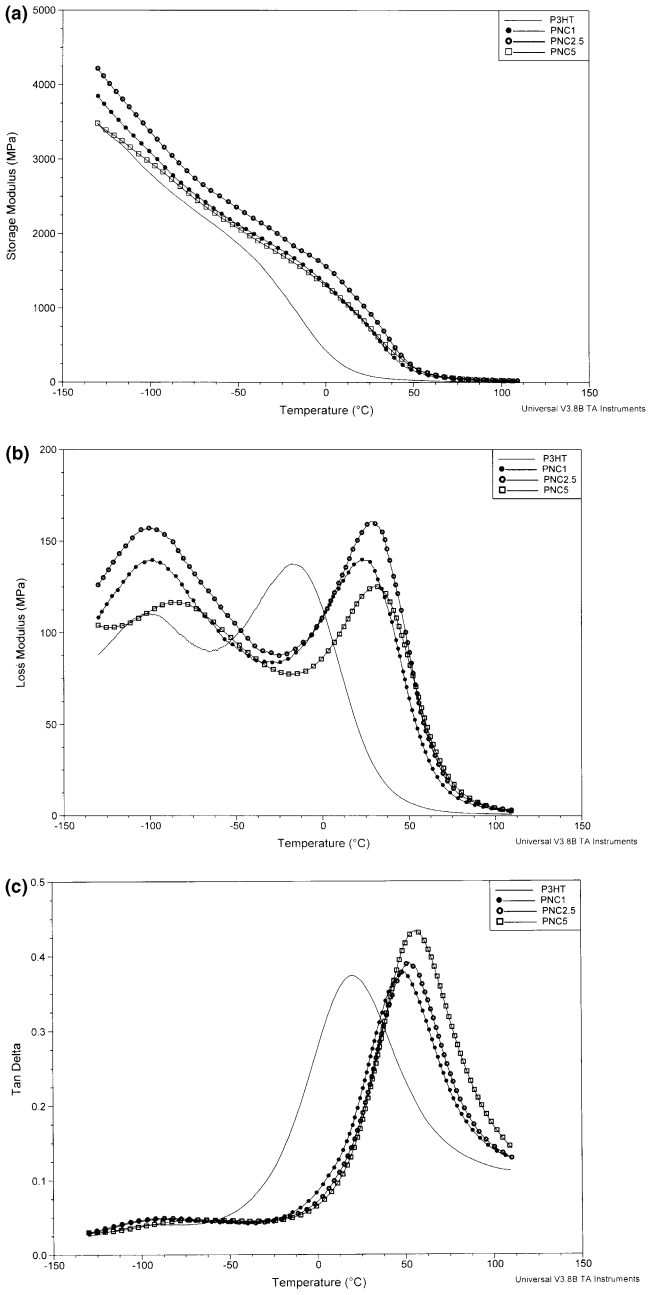

Figure 5. Mechanical property variation of P3HT nanocomposites with temperature: (a) storage modulus; (b) loss modulus; (c) tan δ.

particles on the various relaxation processes of P3HT chain is not quantitatively the same. The induced rigidity of the P3HT main chain is greater than that of the side chain. The latter effect is minimal in the PNC1 and PC2.5 (only 5°), but in the PNC5 the effect is quite large (17°). No definite reason is yet known for this different behavior, and the relative angular disposition of clay platelets on the P3HT strands might be a factor. In tan δ vs temperature plots (Figure 5c) the peak temperature also varies as the α transition peak in loss modulus. The difference between the tan δ peak temperature and loss modulus peak temperature is ∼24 °C for the PNCs, but for the pure P3HT the difference is larger (36 °C). The reason for large difference between tan δ peak and loss modulus peak in the case of P3HT compared to PNCs is not clear. To explain the increase in T_g in the PNCs, a probable explanation that may be

Table 3. Summary of Mechanical Properties of PNCs Measured by DMA

			storage modulus (MPa)					
sample	T_β (°C)[a]	T_g (°C)[a]	−50 °C	(%) increase	20 °C	(%) increase	+50 °C	(%) increase
P3HT	−102.1	−16.0	1863		122.6		29.6	
PNC1	−97.8	25.2	2124	14	859.7	601.2	157.8	433.1
PNC2.5	−98.3	28.2	2341	25.6	1071	773.5	212.2	616.8
PNC5	−84.6	31.7	2074	11.3	875.2	613.8	194.2	556

[a] From loss modulus peaks.

proposed is that the clay platelets attract each other in the dispersed state due to van der Waals attraction causing the P3HT chains to become more close-packed structures, decreasing the free volume. As a result, higher temperature is required to attain the required free volume fraction (0.025) for the onset of segmental Brownian motion,[30] and hence T_gs in the PNCs are increased. Additionally, in the case of intercalated structure the confinement of P3HT chains into the clay lamella may also yield increased T_g value, and the highest T_g value of PNC5 (Table 3) may be attributed for this reason.

The storage modulus (G') values shown in Table 3 clearly indicate that there is a large mechanical reinforcement by the clay particles all over the temperature range for all the PNCs. The nanodimension clay particles for its large surface area and its high aspect ratio show such a large mechanical reinforcement.[31] The enhancement in the modulus appears in different magnitude at different temperature ranges. Below T_g the mechanical reinforcement is lower compared to those at 20 and 50 °C. These results indicate that the effect of clay on mechanical property reinforcement is better in rubbery state than that in the glassy state. In the rubbery state the movement of polymer chain segments is relatively free so the reinforcement effect of clay particles is more effective, causing a larger increase in storage modulus.[4,23] It is apparent from Figure 5a and also from Table 3 that PNC2.5 has the highest storage modulus value than that of the other PNCs. This is probably because of the fact that exfoliated clay structure yields better mechanical property, and the greater the exfoliated clay concentration, the larger is the storage modulus of the sample. PNC2.5 has the greatest exfoliated clay concentration studied here so it showed the highest storage modulus value.

FTIR Spectra. The PNCs are now widely characterized using FTIR spectroscopy.[11,13,32,33] In Figure 6 the FTIR spectra of om-MMT, P3HT, and PNCs are presented. For the om-MMT the bands at 2923, 2851, and 1470 cm^{-1} are for CH_2 asymmetric stretching, symmetric stretching, and in-plane scissoring vibrations, respectively. Silicate-related absorption bands are 1032 cm^{-1} for Si−O−Si stretching and 516 and 463 cm^{-1} for Si−O stretching and Si−O bending, respectively. The 3623 cm^{-1} peak is the absorption band of lattice water (O−H stretching).[33] For P3HT the absorption band at 3054 cm^{-1} is for aromatic CH stretching, 2935 and 2856 cm^{-1} are for aliphatic CH stretching, 1510 and 1457 cm^{-1} are for ring stretching, 1377 cm^{-1} is for the methyl deformation, 820 cm^{-1} is for the aromatic C−H out-of-plane, and 725 cm^{-1} corresponds to the methyl rocking.[34] In the PNCs all the characteristic peaks of om-MMT and P3HT are retained, at lower concentration of the clay intensity of the corresponding peaks are lower, and with increasing om-MMT concentration the intensity of the peaks increases. From the FTIR data it has been noticed that Si−O−Si frequency of om-MMT clay at 1032 cm^{-1} decreased to 1028 and 1029 cm^{-1} for PNC 1 and PNC 2.5 while it increased to 1035 cm^{-1} for PNC 5. We propose that in the exfoliated state the Si−O−Si bonds experience lesser hindrance to vibrate as they are free compared to that in the lamellar state. The increase in Si−O−Si vibration frequency for PNC 5 may be due to the intercalation of P3HT lamella into the clay lamella making the clay lamella structure more compact, shifting the Si−O−Si frequency to a higher value. The same explanation follows for the −Si−O− stretching frequency which occurs at 518, 512, 515, and 518 cm^{-1} for om MMT, PNC 1 PNC 2.5, and PNC5, respectively. In this respect it may also be compared with Na^+-MMT clay where Si−O−Si stretching vibration occurs at 1036 cm^{-1} and Si−O stretching vibration occurs at 520 cm^{-1} due to more compact nature of the lamella.

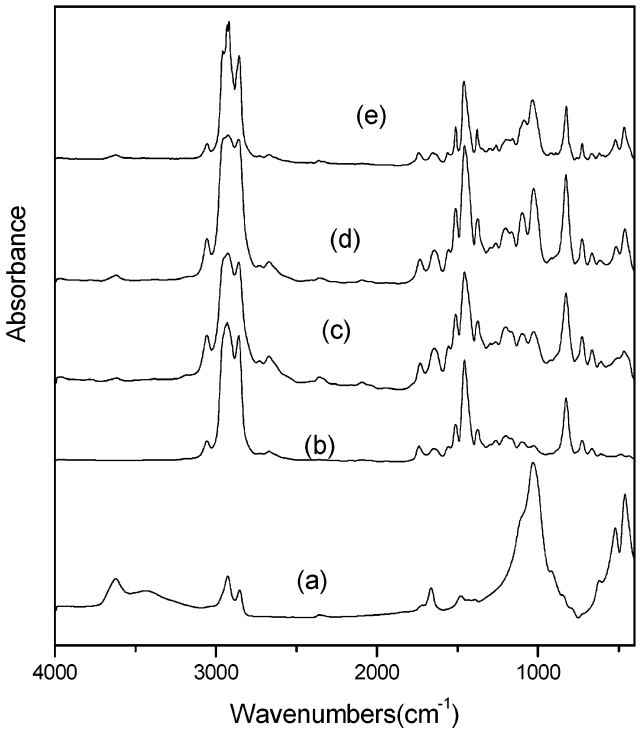

Figure 6. FTIR spectra of P3HT−PNCs: (a) om-MMT, (b) P3HT, (c) PNC1, (d) PNC2.5, and (e) PNC5.

Optical Properties: (a) UV−Vis Absorption Spectra. The UV−vis absorption spectra of P3HT and the PNCs in the solid state are presented in Figure 7. Pure P3HT shows an electronic transition band at 516 nm which may be attributed to the $\pi-\pi^*$ transition of π-conjugated segments of P3HT. In addition, there is a hump at 272 nm which is arises for the $\pi-\pi^*$ transition of thiophene unit.[35] With addition of clay the 516 nm peak shifts to lower wavelength (blue shift). The blue shift is maximum at 2.5% clay content, and it is similar to the blue shift in the UV−vis spectra of cadmium sulfide (CdS) embedded P3HT nanowire.[36] Probably a different structure of P3HT in the composite than that

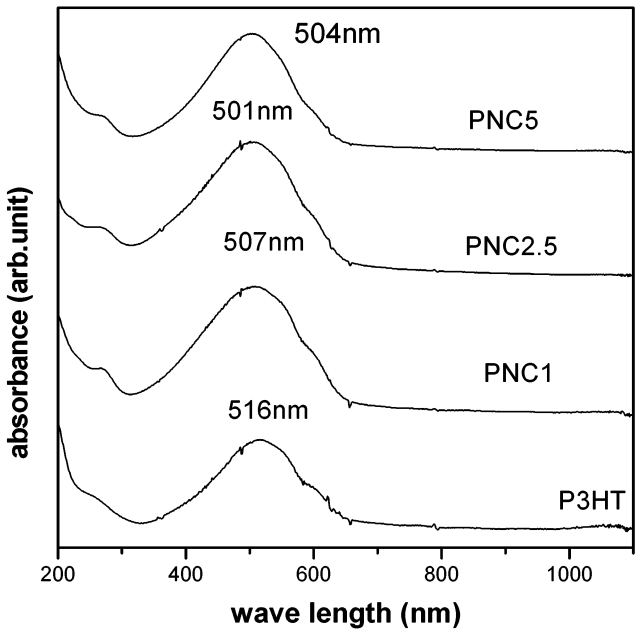

Figure 7. UV−vis spectra of P3HT and PNCs in the solid state at 30 °C.

of pure P3HT may be the reason for its absorption at lower wavelength. It may arise due to both intrachain and interchain mechanisms.[37,38] Intrachain mechanism arises from the backbone conformational change and side group disorder while the interchain mechanism arises from crystallization, gelation, induced rigidity, etc.[37] As T_g is increased in the PNCs so induced rigidity may be an important cause for the short conjugation length due to coiling of the chain, causing the blue shift. Also, the increased crystallinity of PNCs makes the P3HT chains in the compact form which may also be responsible for the blue shift. At the 5% clay content the PNC structure is interlamellar; the clay platelets are not well dispersed, and the crystallinity is lesser compared to that of the PNC2.5. As a result, a decrease in blue shift from that of PNC2.5 is observed at the PNC5.

(b) Photoluminescence Spectra. In Figure 8 the photoluminescence spectra of P3HT and PNCs are compared. It is apparent from the figure that there is photoluminescence quenching in the PNCs, and it increased with increasing clay concentration in the composites. This is an interesting observation and is in sharp contrast to the (MEH−PPV)/clay nanocomposite system where there was an increase of photoluminescence in the PNCs.[18] The observed quenching may be due to rapid charge transfer from the photoexited states. The singlet exiton being dissociated can no longer decay radiatively to the ground state. Another probable reason for the photoluminescence quenching may be due to the energy transfer by Forster mechanism. The overlap of the polymer photoluminescence with the absorption can end the energy transfer with nonradiative decay.

Conductivity. The dc conductivity of both undoped and I_2-doped P3HT and PNC samples is presented in Table 4. It is clear from the table that the conductivity values of undoped samples are almost the same as each other. However, PNC1 has somewhat increased value. There is a blue shift in the UV−vis spectra of PNCs than that of P3HT (Figure 7) but almost same conductivity of them is not in accordance with the spectral observation. Here it is necessary to mention that in the CdS

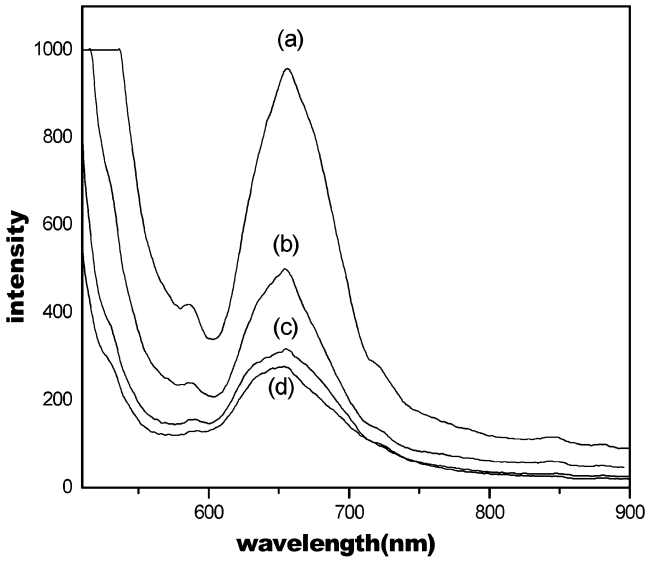

Figure 8. Photoluminescence spectra of P3HT and the PNCs after excitation by radiation of 490 nm wavelength (normalized to film thickness of 1 μm): (a) P3HT, (b) PNC1, (c) PNC2.5, and (d) PNC5.

Table 4. Conductivity Values σ (S/cm) of Undoped and I_2-Doped P3HT and PNCs

sample	undoped	doped
P3HT	6.675×10^{-5}	0.34
PNC1	1.17×10^{-4}	1.15
PNC2.5	7.174×10^{-5}	1.09
PNC 5	7.485×10^{-5}	1.04

embedded P3HT nanowire (showing blue shift) a decrease in conductivity of the nanowire containing film by two orders was observed.[36] A probable reason for this anomalous behavior may be proposed is that the blue shift in UV−vis spectra is mainly due to the intrachain contribution arising due to induced rigidity which increases the band gap of P3HT in the PNCs. As a result, the conductivity should decrease; rather, it remains the same. Probably, the increased interchain part of conductivity arising from the increased interchain contacts due to induced rigidity compensates for the intrachain contribution. The increased interchain contact may also be responsible for the decrease in photoluminescence efficiency of the PNCs as it helps for the rapid charge transfer from the photoexited state. In the iodine-doped samples, the conductivity of PNCs are 2.5−3 times larger than that of pure P3HT. It is really an interesting observation, and no definite reason can be afforded at present. So it is possible to get PNCs of P3HT where conductivity is fully retained, and in the doped system it is improved. The mechanical properties and thermal stability are highly improved compared to that in the pure polymer. Such PNCs may therefore find use in various electronic and optoelectronic applications.

Conclusion. P3HT produces nanocomposite with organically modified MMT clay when cast from chloroform. At lower clay content the clay has exfoliated structure, but at higher clay content (5%) it has lamellar structure as evidenced from WAXS and TEM studies. The interchain lamella of P3HT exists in the nanocomposite, and the P3HT crystals become more ordered, showing better Xray diffraction peaks. The melting point and enthalpy of fusion of P3HT are increased in the PNCs; so also are the β-transition temperature and glass transition temperature. The storage modulus of

PNCs increased greatly than that of pure polymer. The FTIR study indicates a decrease in Si−O−Si and Si−O stretching frequency for the exfoliated clay structure. UV−vis study shows a blue shift in the spectra of PNCs, and photoluminescence quenching occurs in the PNCs. The conductivity values of undoped samples remain unaffected, but iodine-doped PNCs however exhibit 2.5−3 times increase in conductivity.

Acknowledgment. We gratefully acknowledge the Council of Scientific and Industrial Research (Grant 01-(1919)/04/EMR -II), New Delhi, for financial support. Also, the financial help from Department of Science and Technology under Nano Science and Nano Technology Program is gratefully acknowledged.

Supporting Information Available: Figures of TGA curves of Na^+−MMT clay and MMT clay and micrographs of PNC2.5 and PNC5. This material is available free of charge via the Internet at http://pubs.acs.org.

References and Notes

(1) McCullough, R. D.; Ewbank, P. C. In *Handbook of Conducting Polymers*, 2nd ed.; Skotheim, T. A., Elsebaumer, R. L., Reynolds, J. R., Eds.; Marcel Dekker: New York, 1998; p 225.
(2) Vaia, R. A.; Krishnamoorti, R. In *Polymer Nanocomposites: Synthesis Characterization and Modeling*; Krishnamoorti, R., Vaia, R. A., Eds.; American Chemical Society: Washington, DC, 2001; p 1.
(3) Maiti, P.; Nam, P. H.; Okamoto, M.; Hasegawa, N.; Usuki, A. *Macromolecules* **2002**, *35*, 2042.
(4) Sinha Ray, S.; Maiti, P.; Okamoto, M.; Yamada, K.; Ueda, K. *Macromolecules* **2002**, *35*, 3104.
(5) Giannelis, E. P.; Krishnamoorty, R.; Manias, E. *Adv. Polym. Sci*. **1999**, *138*, 107.
(6) Park, J. H.; Jana, S. C. *Macromolecules* **2003**, 36, 2758, 8391.
(7) Alxandre, M.; Dubois, P. *Mater. Sci. Eng. Rev.* **2000**, *R28* (1−2), 1.
(8) Yano, K.; Usuki, A.; Okada, A. *J. Polym. Sci., Polym. Chem.* **1997**, *35*, 2289.
(9) Zhu, J.; Morgan, A. B.; Lamelas, F. J.; Wilkie, C. A. *Chem. Mater.* **2001**, *13*, 3774.
(10) Prosa, T. J.; Winokur, M. J.; McCullough, R. D. *Macromolecules* **1996**, *29*, 3654.
(11) Yeh, J.-M.; Liou, S.-J.; Lai, C.-Y.; Wu, P.-C.; Tsai, T.-Y. *Chem. Mater*. **2001**, *13*, 1131.
(12) Lee, D.; Char, K.; Lee, S. W.; Park, Y. W. *J. Mater. Chem.* **2003**, *13*, 2942.
(13) do Nascimento, G. M.; Constantino, V. R. L.; Temperini, M. L. A. *Macromolecules* **2002**, *35*, 7535.
(14) Kim, B. H.; Jung, J. H.; Kim, J. W.; Choi, H. J.; Joo, J. *Synth. Met.* **2001**, *117*, 115.
(15) Wu, Q.; Xue, Z.; Qi, Z.; Wang, F. *Polymer.* **2000**, *41*, 2029.
(16) Feng, B.; Su, Y.; Song, J.; Kong, K. *J. Mater. Sci., Lett.* **2001**, *20*, 293.
(17) Liu, Y.-C.; Tsai, C.-J. *Chem. Mater.* **2003**, *15,* 320.
(18) Lee, T.-W.; Park, O. O.; Kim, J.-J.; Hong, J.-M.; Kim, Y. C. *Chem. Mater.* **2001**, *13,* 2217.
(19) Roncali, J. *Chem. Rev.* **1992**, *92*, 711.
(20) Pal, S.; Nandi, A. K. *Macromolecules* **2003**, *36*, 8426.
(21) Amou, S.; Haba, O.; Shirato, K.; Hayakawa, T.; Ueda, M.; Takeuchi, K.; Asai, M. *J. Polym. Sci., Polym. Chem.* **1999**, *37*, 1943.
(22) Yeh, J.-M.; Liou, S.-J.; Lin, C.-Y.; Cheng, C.-Y.; Chang, Y.-W.; Lee, K.-R. *Chem. Mater.* **2002**, *14*, 154.
(23) Usuki, A.; Kawasumi, M.; Kujima, Y.; Okada, A.; Kurauchi, T.; Kamigaito, O. *J. Mater. Res.* **1993**, *8*, 1185.
(24) Frommer, J. E.; Chance, R. R. In *Encyclopedia of Polymer Science and Engineering*, 2nd ed.; Mark, H. F., Bikales, N. M., Overberger, C. G., Menges, G., Eds.; John Wiley and Sons: New York, 1986; Vol. 5, p 473.
(25) Maiti, P.; Yamada, K.; Okamoto, M.; Ueda, K.; Okamoto, K. *Chem. Mater.* **2002**, *14*, 4654.
(26) Tashiro, K.; Ono, K.; Minagawa, Y.; Kobayashi, M.; Kawai, T.; Yoshino, K. *J. Polym. Sci.* **1991**, *B29*, 1223.
(27) Mena-Osteritz, E.; Meyer, A.; Langeveld-Voss, B. M. W.; Janssen, A. J. R.; Meijer, E. W.; Bauerle, P. *Angew. Chem., Int. Ed.* **2000**, *39*, 2680.
(28) Ferry, J. D. *Viscoelastic Properties of Polymers*; John Wiley and Sons: New York, 1961.
(29) Heijboer, J. *J. Polym. Sci.* **1968**, *C16*, 3755.
(30) Kovacs, A. J. *Adv. Polym. Sci.*. **1963**, *3*, 394.
(31) Okamoto, M.; Morita, S.; Kim, Y. H.; Kotaka, T.; Tateyama, H. *Polymer* **2001**, *42*, 1201.
(32) Zeng, Q. H.; Wang, D. Z.; Yu, A. B.; Lu, G. Q. *Nanotechnology* **2002**, *13*, 549.
(33) Darder, M.; Colilla, M.; Ruiz-Hitzky, E. *Chem. Mater*. **2003**, *15*, 3774.
(34) Chen, T.-A.; Wu, X.; Rieke, R. D. *J. Am. Chem. Soc.* **1995**, *117*, 233.
(35) Liu, Y.; Xu, Y.; Zhu, D. *Macromol. Chem. Phys.* **2001**, *202*, 1010.
(36) Malik, S.; Batabyal, S. K.; Basu, C.; Nandi, A. K. *J. Mater. Sci., Lett* **2003**, *22*, 1113.
(37) Rughooputh, S. D. D. V.; Hotta, S.; Heeger, A. J.; Wudl, F. *J. Polym. Sci., Part B: Polym. Phys.* **1987**, 1071.
(38) Malik, S.; Jana, T.; Nandi, A. K. *Macromolecules* **2001**, *34*, 275.

MA0490496